PAPER

Sensitized ZnO nanorod assemblies to detect heavy metal contaminated phytomedicines: spectroscopic and simulation studies†

Damayanti Bagchi,[a] Tuhin Kumar Maji,[a] Samim Sardar,[a] Peter Lemmens,[bc] Chinmoy Bhattacharya,[d] Debjani Karmakar[e] and Samir Kumar Pal*[a]

The immense pharmacological relevance of the herbal medicine curcumin including anti-cancer and anti-Alzheimer effects, suggests it to be a superior alternative to synthesised drugs. The diverse functionalities with minimal side effects intensify the use of curcumin not only as a dietary supplement but also as a therapeutic agent. Besides all this effectiveness, some recent literature reported the presence of deleterious heavy metal contaminants from various sources in curcumin leading to potential health hazards. In this regard, we attempt to fabricate ZnO based nanoprobes to detect metal conjugated curcumin. We have synthesized and structurally characterized the ZnO nanorods (NR). Three samples namely curcumin (pure), Zn–curcumin (non-toxic metal attached to curcumin) and Hg–curcumin (toxic heavy metal attached to curcumin) were prepared for consideration. The samples were electro-chemically deposited onto ZnO surfaces and the attachment was confirmed by cyclic voltammetry experiments. Moreover, to confirm a molecular level interaction picosecond-resolved PL-quenching of ZnO NR due to Förster Resonance Energy Transfer (FRET) from donor ZnO NR to the acceptor curcumin moieties was employed. The attachment proximity of ZnO NR and curcumin moieties depends on the size of metals. First principles analysis suggests a variance of attachment sites and heavy metal Hg conjugated curcumin binds through a peripheral hydroxy group to NR. We fabricated a facile photovoltaic device consisting of ZnO NR as the working electrode with Pt counter electrode and iodide–triiodide as the electrolyte. The trend in photocurrent under visible light illumination suggests an enhancement in the case of heavy metal ions due to long range interaction and greater accumulation of charge at the active electrode. Our results provide a detailed physical insight into interfacial processes that are crucial for detecting heavy-metal attached phytomedicines and are thus expected to find vast application as sensors for the detection of selective metal contaminants.

[a] *Department of Chemical, Biological and Macromolecular Sciences, S. N. Bose National Centre for Basic Sciences, Block JD, Sector III, Salt Lake, Kolkata 700 106, India. E-mail: skpal@bose.res.in; Fax: +91-033-2335-3477; Tel: +91-033-2335-5706-08*

[b] *Institute for Condensed Matter Physics, TU Braunschweig, Mendelssohnstraße 3, 38106 Braunschweig, Germany*

[c] *Laboratory for Emerging Nanometrology, TU Braunschweig, 38106 Braunschweig, Germany*

[d] *Department of Chemistry, Indian Institute of Engineering Science and Technology Shibpur, P.O. Botanic Garden, Howrah-711103, India*

[e] *Technical Physics Division, Bhaba Atomic Research Centre, Mumbai 400085, India*

† Electronic supplementary information (ESI) available. See DOI: 10.1039/c6cp08016b

1. Introduction

Herbal medicines with a rich polyphenol content are attracting interest and are sometimes even preferred with respect to synthesised drugs due to their multiple functionalities, reduced side effects and cost-effectiveness.[1,2] The rising use of herbal medicines suggests that attention should be paid to the paramount issue of quality as it is directly related to safety and efficacy of the medicines.[3] The introduction of chemical toxins such as harmful pesticides, non-essential heavy metals (as Cd, Hg, Pb *etc.*) into these plant materials during harvesting or post-harvest collection and storage can lead to therapeutically less effective agents with some adverse action.[4] However, plants can execute some superficial mechanisms by forming metal–ligand complexes in the rhizosphere which can limit the uptake of metals by roots and help plants to tolerate a certain amount of toxic metals in the soil.[5]

Turmeric, the golden yellow spice of India, is considered to be one of the most efficacious herbal plants due to its prolific content of natural phenols such as curcuminoids.[6] Curcumin is the principal curcuminoid of turmeric and used to be isolated from rhizomes of *Curcuma longa*.[7] Besides the popularity of

This journal is © the Owner Societies 2017

Phys. Chem. Chem. Phys., 2017, **19**, 2503–2513 | 2503

curcumin as a spice, it exhibits varieties of medicinal applications including the use as an anticancer agent,[8,9] anti-Alzheimer's agent,[10] and anti-Parkinson's disease neuroprotective agent,[11] which emphasizes its significance as a herbal medicine. The behaviour of curcumin as a chelating ligand to bivalent metal ions such as zinc, copper, manganese, iron leading to the formation of metallo-curcumin complexes enhances both the solubility and activity of curcumin.[12–15] Our recent report suggested enhancement of solubility and stability of curcumin in aqueous media *via* metallation using Zn(II) and the successional replacement of Zn(II) in the complex by Cu(II) through a simple route can increase the activity prior to its use.[16] But this ligation property of curcumin has some contrasting effect as it can effectively chelate heavy metal ions[17] such as cadmium, lead, mercury, and arsenic. In a recent literature, it has been reported that contaminated curcumin can be a potential source of lead exposure.[18] Chronic exposure to curcumin may cause elevated blood lead levels (BLL) as it contains extremely high bio-accessible lead levels.[19] It is more alarming that this lead contamination affects children mostly due to high gastrointestinal uptake and the permeable blood–brain barrier.[20] The dietary supplement curcumin might contain elevated levels of mercury and arsenic contamination also.[21] Moreover turmeric is profoundly used in cosmetics and applying the metal contaminated turmeric directly to the skin enhances the possibility of metal contamination in the body.[22] This necessitates the urgent requirement of a facile detection procedure for heavy metal conjugated curcumin. However, to date no such attempt has been made, except using conventional techniques.[23]

Herein, we propose the use of ZnO nanorods (NR) for differentiating between pure curcumin (Cur) and metal attached curcumin (M–Cur). We have synthesized ZnO NR[24] which is environment friendly and is less toxic than other semiconductor oxides[25] and its structural characterization was performed. In order to detect Cur and M–Cur distinctly, we have used Cur (as the pure sample), synthesized Zn–Cur (as non-toxic M–Cur), and Hg–Cur (as toxic M–Cur). The samples are electrochemically deposited covering ZnO NR surfaces. The intrinsic defect state emission of the ZnO NR and its spectral overlap with the absorption spectrum of Cur and M–Cur samples reveals Förster Resonance Energy Transfer (FRET) from the surface of the NR to the attached moieties, confirming the close proximity between them. The variance in FRET distances for different samples suggest that Cur and M–Cur are attached to the ZnO NR surface through different binding sites. First principles analysis of ground-state energies unveils that for Cur and Zn–Cur, the NRs are attached through keto–enolic sites, whereas for Hg–Cur the attachment is through the *o*-methoxy phenolic site. This result motivated us to fabricate a photovoltaic device using ZnO NRs sensitized with Cur or M–Cur as the active electrode to measure the photocurrent under visible light irradiation. The trend in photocurrent clearly shows an immense disparity suggesting that an electron recombination process is active in Cur and Zn–Cur systems which gets hindered for the Hg–Cur sample. The slow back electron transfer process from the active layer (consisting of Hg–Cur)

to the electrolyte justifies the observed photocurrent trend. To envisage the detailed mechanism responsible for the contrasting experimental behaviour of these samples, we have investigated the electronic structure of Cur-NR, Zn–Cur-NR and Hg–Cur-NR with the help of density functional calculations. Our study offers a detailed physical insight and motivation for using ZnO NR as nanoprobes to characterize heavy-metal conjugated curcumin and is thus expected to find relevance in the large scale, for daily consumer based applications.

2. Experimental section

2.1. Materials

In this study analytical grade chemicals were used for the synthesis without further purification. Curcumin, $Zn(OAc)_2·2H_2O$, $Hg(NO_3)_2·H_2O$, zinc nitrate hexahydrate $Zn(NO_3)_2·6H_2O$ and hexamethylenetetramine $C_6H_{12}N_4$ were purchased from Sigma-Aldrich. Methanol (Merck) was used as a suitable solvent to synthesise M–Cur complexes. For all other studies, Cur and M–Cur complexes were dissolved in dimethyl sulfoxide (DMSO, from Merck). Fluorine-doped tin oxide (FTO) conducting glass substrates were acquired from Sigma-Aldrich and were cleaned by successive sonication with acetone, deionized (DI) water and ethanol, each for 15 min, with proper drying prior to the final use.

2.2. Synthesis of ZnO NRs

Zinc acetate dihydrate $Zn(OAc)_2·2H_2O$, zinc nitrate hexahydrate $Zn(NO_3)_2·6H_2O$, and hexamethylenetetramine $C_6H_{12}N_4$ were used as the starting materials for a low temperature hydrothermal synthesis of ZnO NRs on FTO substrates. The details of the hydrothermal growth of ZnO NRs are described in our previous reports.[24,26–28] Finally, ZnO NRs of length 2–3 μm and diameter 80–100 nm were synthesized.

2.3. Synthesis of M–Cur complexes

2.3.1. Zn(II)–Cur complex. 50 mL 2 mM methanolic solution of curcumin was prepared by stirring and heating at 60 °C. Zinc acetate dihydrate (2 mM) was dissolved in 100 mL methanol by heating and the solution was added into the curcumin. The immediate formation of a red precipitate confirms the complexation reaction. The reaction mixture was refluxed at 180 °C for 2 h. The red solid product was filtered and washed firstly by cold methanol and then by water to remove the residue reactants.[29] The purified product was dried in a vacuum overnight and the final appearance of the product was a red crystalline powder. The synthesized product exhibits 1 : 1 stoichiometric ratio of Zn(II) and curcumin as reported in the earlier literature.[16]

2.3.2. Hg(II)–Cur complex. This complex was synthesized using the above described procedure only by changing the acetate salt to $Hg(NO_3)_2·H_2O$. The Hg(II)–Cur[30] was obtained as a brown crystalline powder.

2504 | *Phys. Chem. Chem. Phys.,* 2017, **19**, 2503–2513

This journal is © the Owner Societies 2017

2.4. Electrochemical deposition of Cur and M–Cur complexes on ZnO NRs

A stock solution of 1 mM Cur and 1 mM M–Cur was prepared in DMSO and complete dissolution of the solid was ensured by subsequent cyclo-mixing and sonication. 200 μL of the stock solution of Cur or M–Cur is added into 50 mL phosphate buffer solution (PBS) containing 5 g of KCl. To this solution, FTO plate with the grown ZnO NR was dipped, which acts as the working electrode. A Pt counter electrode was used with an Ag/Ag$^+$ reference couple. The dipped solution was electrochemically deposited applying an open circuit potential method using a potential range of −2 to +2 volts for a time window of 4 h with consecutive monitoring of the deposition by cyclic voltammetry (CV) initially and at an interval of 2 h. Finally after 4 h of deposition, the plates were taken out of the solution, washed with PBS several times and analysed using CV and spectroscopic methods.

2.5. Characterization methods

For optical characterization a Shimadzu UV-2600 spectrophotometer was employed to measure absorption spectra using a quartz cell of 1 cm path length. Steady-state fluorescence measurements were performed using a JobinYvon Fluorolog fluorometer. The steady state emissions of all samples were taken upon excitation at the wavelength of 430 nm. The fluorescence measurements were performed with the excitation and emission bandwidth slits at 5 nm. The corresponding excitation spectra were monitored at the emission wavelength of 550 nm keeping both slit widths at 5 nm. For structural characterization, a scanning electron microscopy (SEM) system (QUANTA FEG 250) was used to study the morphology of ZnO NRs. Transmission electron microscopy (TEM) grids were prepared by applying a diluted drop of ZnO NR sample solution onto carbon coated copper grids. The particle sizes were determined from micrographs recorded at a magnification of 100 000× using an FEI microscope (Tecnai S-Twin, operating at 200 kV). Powder X-ray diffraction (XRD) patterns were in the 2θ range from $20°$ to $80°$ using a PANalytical XPERT-PRO diffractometer equipped with Cu Kα radiation (at 40 mA, 40 kV). Electrochemical experiments were performed using a CH analyser potentiostat (CHI1110C). For cyclic voltammetry, a three electrode system consisting of ZnO NRs on FTO plates as the working electrode, a platinum counter electrode and a reference electrode of the Ag/Ag$^+$ couple was employed. For deposition onto ZnO NRs surface, Cur and M–Cur were used as the electrolyte solution whereas for CV measurements PBS solution containing KCl was used as electrolyte solution. Time-resolved studies were performed using a time-correlated single-photon counting (TCSPC) setup from Edinburgh Instruments. A picosecond pulsed laser diode was used to excite the sample at 375 nm with an instrument response function (IRF) of 75 ps. The excitation was vertically polarized, and the emission was recorded through a polarizer oriented at $55°$ from the vertical position. Incorporation of a long-pass filter with a cut-off at 420 nm in the emission channel effectively eliminates possible scattered excitation light.

The picosecond resolved fluorescence transients were fitted with multiexponential function.[31] The details of the picosecond time resolved FRET studies and the parameters involved in the equations are described in earlier reports.[32,33] From the average lifetime calculations for the samples, we obtain the effective distance between the donor and the acceptor (r_{DA}).[34,35]

2.6. Fabrication of a photovoltaic device for photocurrent measurements

Photocurrent measurements were carried out in a photovoltaic device set up under 1 sun condition. The platinum (Pt) nanoparticles were deposited on the FTO substrates via thermal decomposition of 5 mM platinum chloride, $H_2PtCl_6\cdot H_2O$ (Sigma-Aldrich) solution in isopropanol at 385 °C for 30 min. This is used as the counter electrode. Cur or M–Cur sensitized ZnO NR was used as the active electrodes and the two electrodes were placed on top of each other with a single layered 60 μm thick Surlyn (Solaronix) as a spacer between the two electrodes. Cur and M–Cur solution were deposited on the ZnO NRs following the same electrochemical method. A liquid electrolyte composed of 0.5 M lithium iodide (LiI), 0.05 M iodine (I_2) and 0.5 M 4-tertbutylpyridine (TBP) in acetonitrile was used as the hole conductor and filled in the inter-electrode space by using capillary force, through two small holes (diameter = 1 mm) pre-drilled on the counter electrode. Finally, the two holes were sealed by using another piece of Surlyn to prevent the leakage of the electrolyte from the cell. In all our experiments, the active area was fixed at 1 cm^2. Electrochemical impedance spectroscopy (EIS) was performed on an electrochemical workstation CHI650E (CH instruments) with a frequency range from 100 kHz to 0.1 Hz under the open circuit conditions. All impedance measurements were carried out under a bias illumination of 100 mW cm^2. The obtained spectra were fitted using the CHI650E software in terms of appropriate equivalent circuits. Photovoltage decay measurements were carried out after illumination of the device under 1 sun conditions and were monitored by an oscilloscope (Owon) through a computer interface. The decays were fitted with exponential decay functions using Origin software (Origin Lab).

3. Computational details

For density functional calculations, we have used projector augmented wave (PAW) potentials under generalized gradient approximation (GGA) with Perdew–Burke–Ernzerhoff exchange correlation functional as implemented in the Vienna ab initio simulation package (VASP).[36] The plane wave cut-off energy was set to 500 eV. All control and assembled systems are placed in a rectangular box of dimension $\sim 30 \times 20 \times 20$ Å^3, with sufficient vacuum so as to avoid influence from periodic replication. Due to a large volume of the simulation cell for these cluster systems, single k-point (Γ point) calculations are performed for these systems with ionic optimization under conjugate gradient algorithm until the Hellmann–Feynmann force on

This journal is © the Owner Societies 2017

Phys. Chem. Chem. Phys., 2017, **19**, 2503–2513 | **2505**

each ion is less than 0.01 eV Å^{-1}. van der Waals corrections are incorporated in this calculation using the Grimme DFT-D2 formalism.[37]

4. Results and discussion

The SEM images of the synthesized nanoprobe ZnO NR are shown in Fig. 1a top view and 1b side view. The ZnO NRs are found to be 2–3 μm in length and have diameters of 80–100 nm. The typical hexagonal surface of the NRs is shown in the inset of Fig. 1a. A high-resolution transmission electron microscopic (HR-TEM) image of ZnO NR clearly depicts lattice fringes consisting of an inter-planar distance of 0.338 nm (Fig. S1 in the ESI†), corresponding to the spacing between two (100) planes.[24]

The XRD pattern (Fig. S2 in the ESI†) is also consistent with the previous literature.[24] The synthesized Cur and M–Cur exhibit absorption in the region 430 nm in DMSO as shown in Fig. 1c. Curcumin shows an absorption peak at 430 nm due to an electronic transition which is typically π–π* in nature. After the successful attachment of the metal to curcumin, the absorption spectra change slightly. In the case of Zn–Cur, the main peak is observed at 430 nm with a shoulder at around 454 nm. The change in absorption spectra might be correlated with the formation of a new charge-transfer state by an electronic transition from the ligand curcumin to the metal ion. Hg–Cur shows a slight blue shift in the UV-Vis spectra with a peak maximum at 422 nm (Fig. 1c). The inset depicts the emission spectra of Cur and M–Cur having similar OD at 430 nm, revealing a broader peak near 540 nm upon excitation at
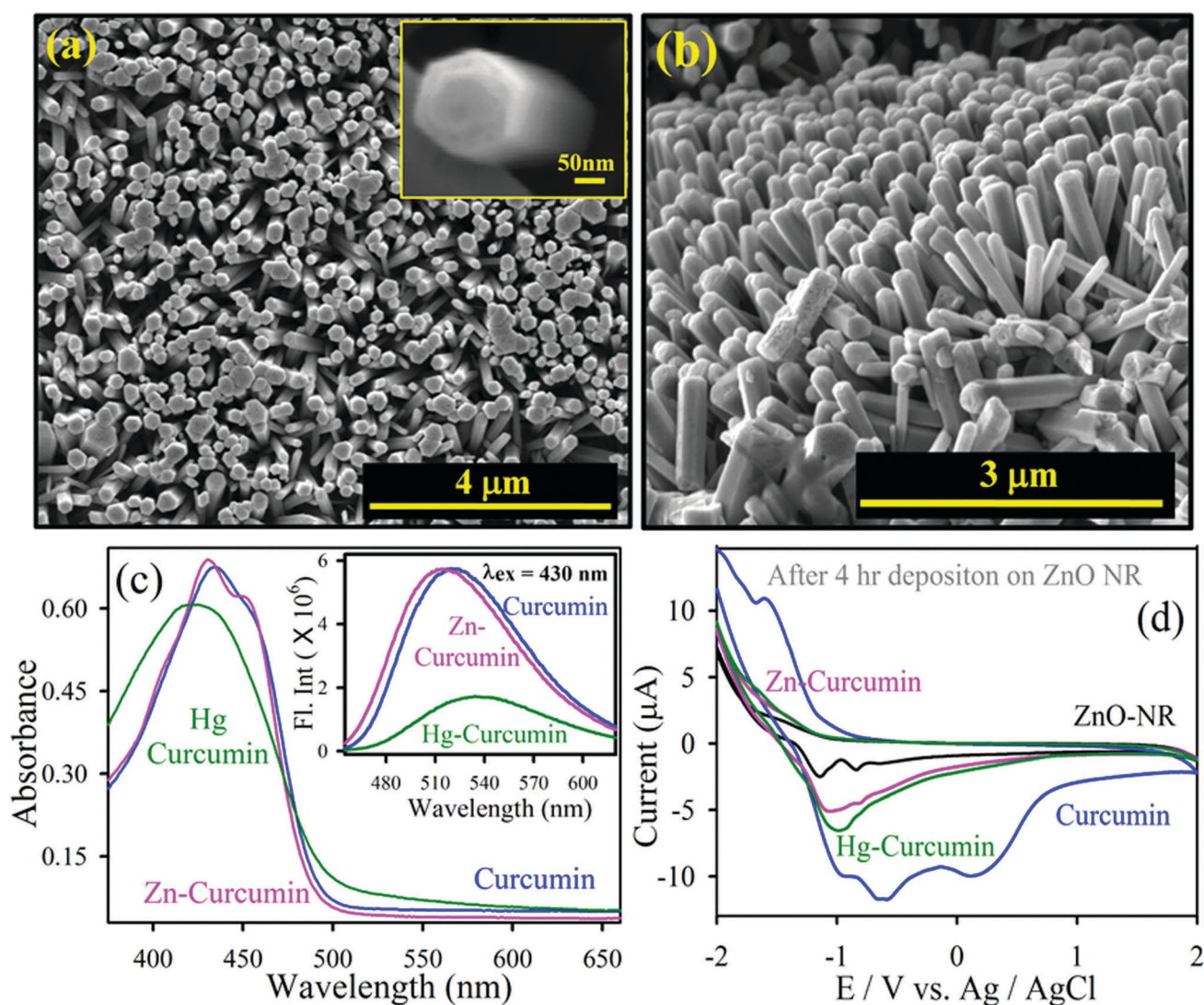

Fig. 1   (a) FEG-SEM of the ZnO nanorods (ZnO NR) on a glass plate. Inset shows magnified image of nanorod. (b) Side view of ZnO NRs. (c) Absorption spectra of curcumin (blue), Zn–curcumin (pink), Hg–curcumin (dark green) in DMSO. Inset depicts emission spectra of curcumin (blue), Zn–curcumin (pink), Hg–curcumin (dark green) in DMSO. The excitation wavelength is 430nm. (d) Cyclic voltammograms of curcumin (blue), Zn–curcumin (pink), Hg–curcumin (dark-green) after 4 h open circuit deposition onto ZnO-NR fabricated on FTO plates. CV measurements were performed in PBS-aqueous KCl solution at a 0.8 V s^{-1} scan rate and Ag/AgCl as a reference electrode.

2506 | *Phys. Chem. Chem. Phys.*, 2017, **19**, 2503–2513

This journal is © the Owner Societies 2017

430 nm. We have measured the excitation spectra while the emission is monitored at 550 nm. Cur shows a broad peak between 420 and 440 nm and after metallation with Zn, there are two peaks at 430 nm and 454 nm whereas Hg–Cur shows a broad band from 420 nm to 450 nm (Fig. S3 in the ESI†). Although there are changes in optical properties between Cur and M–Cur, these differences are not sufficient to distinctly detect the presence of metal conjugated curcumin. In order to investigate the attachment of the Cur and M–Cur by electrochemical deposition to ZnO NR surface, cyclic voltammetry experiments were performed at different time intervals – initial, after 2 h and after 4 h of deposition. Fig. 1d shows comparative voltammograms after 4 h of deposition. The deposition of Cur

or M–Cur onto the surfaces of the ZnO NRs significantly alters the interfacial charge transfer processes and greatly affects their electrochemical properties.[38] As evident from previous reports, electro-oxidation of curcumin follows two consecutive steps via multiple intermediate formations which are essentially pH dependent. In the first step, a phenolic hydroxyl group of curcumin is oxidized via formation of a stable phenoxy radical at a peak 0.6 V followed by its conversion to quinone at 0.3 V.[39] The peak near 0.95 V might be correlated with oxidation of an enolic hydroxyl group.[40] In the case of Cur attached ZnO, the peaks are at 0.25 V, 0.63 V and 0.98 V which are in accordance with the peak value of free curcumin. The redox potentials can be attributed to the binding of curcumin at
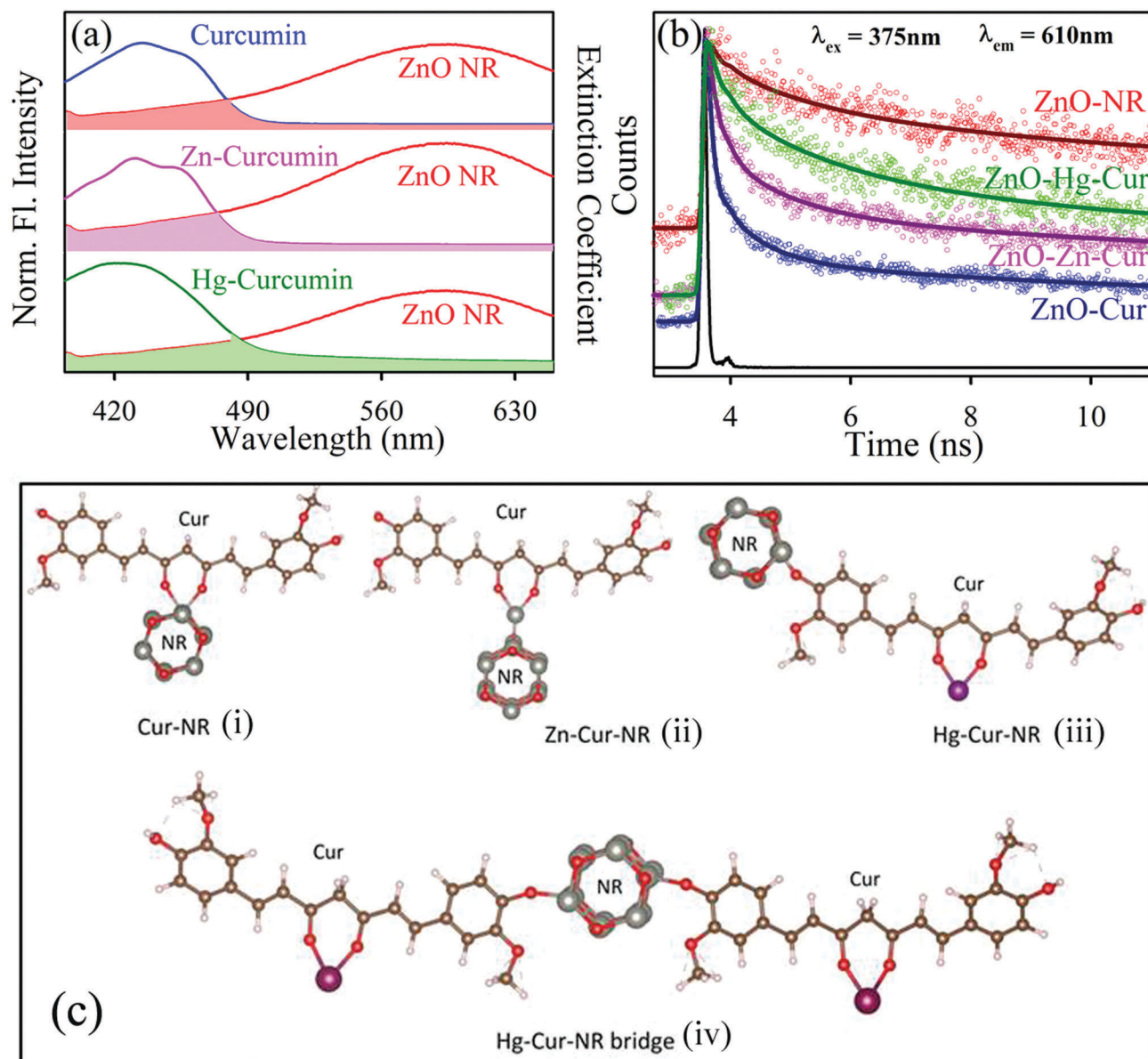

Fig. 2 (a) Spectral overlaps of the emission of ZnO NRs and the absorption spectrum of curcumin (red), Zn–curcumin (pink), Hg–curcumin (green) are shown. (b) Picosecond resolved emission transients of ZnO NRs and composite systems, detected at 610 nm. (c) Schematic ground state configuration of different structures (i) Cur-NR (ii) Zn–Cur-NR (iii) Hg–Cur-NR (iv) Hg–Cur-NR (bridge).

the ZnO surface. The M–Cur attached ZnO NRs depict a smaller (Zn–Cur – 0.98 V and Hg–Cur – 0.90 V) shift compared to curcumin, demonstrating lower affinity towards attachment. The well-documented FTIR spectra of ZnO–Cur illustrate the attachment between the two moieties but the specific site of attachment is not properly recognized.[41]

To illustrate the feasibility of attachment of ZnO NR and Cur or M–Cur, we employed a FRET based spectroscopic method. The synthesized NR surfaces were observed to emit at 590 nm due to the presence of intrinsic oxygen vacancies.[42] The broad NR emission is composed of two bands: a doubly charged vacancy centre (V_O^{++}) located at 610 nm (P_2), a singly charged vacancy centre (V_O^{+}) located at 550 nm (P_1).[43,44] Fig. 2a illustrates the significant spectral overlap between emission of donor ZnO NR and absorption of acceptor Cur or M–Cur. The estimation of distances between two molecular units from FRET based calculations is extremely useful for many assignments.[45] The fluorescence decay profiles of the donor ZnO NR in the presence and absence of the acceptors Cur or M–Cur were measured (Fig. 2b) upon excitation with 375 nm laser and monitored at 610 nm (P_2).[46] The excited-state lifetime of the ZnO NRs quenches after binding with Cur or M–Cur compared to that of bare ZnO NRs. In the case of Cur, the quenching is maximum followed by that for Zn–Cur and Hg–Cur. The details of the lifetime data with their relative contribution in the fluorescence decays are tabulated in Table 1. From FRET calculations (Table 2), the distance between the donor ZnO NR and

Table 1 Picosecond-resolved fluorescence transient lifetime

System	τ_1 (ns)	τ_2 (ns)	τ_3 (ns)	τ_{avg} (ns)
ZnO NR	0.20 (23%)	1.73 (26%)	22.0 (51%)	11.70
ZnO–curcumin	0.08 (73%)	0.72 (15%)	13.9 (11%)	1.70
ZnO–Zn–curcumin	0.25 (59.8%)	1.80 (16.5%)	18.0 (23.7%)	4.70
ZnO–Hg–curcumin	0.23 (35%)	1.95 (28%)	20.0 (37%)	7.90

The emission (monitored at 610 nm) was detected with 375 nm laser excitation. Numbers in parentheses indicate relative contributions.

Table 2 FRET parameters

System	$J(\lambda)$	R_0 (Å)	E	r_{DA} (nm)
ZnO–curcumin	0.497×10^{15}	13.80	0.854	1.03
ZnO–Zn–curcumin	0.48×10^{15}	13.72	0.596	1.27
ZnO–Hg–curcumin	0.69×10^{15}	14.57	0.320	1.66

Table 4 Lowest distances between the two moieties, calculated theoretically

System	Lowest distance between two moieties (Å)
Cur-NR	2.0
Zn–Cur-NR	1.9
Hg–Cur-NR	3.6
Hg–Cur-NR-bridge	3.6

acceptors Cur, Zn–Cur and Hg–Cur is found to be 1.0 nm, 1.3 nm and 1.7 nm, respectively. The energy transfer efficiency is calculated to be 85.4%, 59.6% and 32% for Cur, Zn–Cur and Hg–Cur, respectively. These results suggest a molecular level interaction between ZnO NR and Cur or M–Cur. The distance between M–Cur and ZnO NRs significantly increased with increase in the size of the metal ions, which indicates the possibility of a non-identical binding site for different systems. Thus we have explored the ground state energy stability of four experimental control systems, *viz.*, ZnO nanorods (NRs), pristine curcumin (Cur), Zn–curcumin (Zn–Cur) and Hg–curcumin (Hg–Cur), which indicates that the pristine system is energetically most stable (Table 3). The formation of M–Cur complexes materializes *via* the diketo moiety, which acts as a chelating agent for complexation with metal ions.[12] For the formation of the NR attached complexes, depending upon the Cur system, there are two possible attachment sites. The NR may be chelating through the middle diketo site or *via* the o-methoxy phenolic group at the end of the Cur chain. A comparison of the ground-state energies obtained from theoretical calculations unveils that for Cur and Zn–Cur, NR is attached through the keto–enolic site, whereas for Hg–Cur the attachment is through the o-methoxy phenolic site. Interestingly, for Hg-Cur-NR assembly, there is an even lower-energy symmetric configuration, where two Hg–Cur chains get attached to the two opposite sides of NR (Fig. 2c(iv)), which will be referred as Hg-bridge. These energetically favourable ground state configurations, as suggested from our theoretical calculations, are depicted in Fig. 2c. Table 3 presents the number of atom-normalized total-energy, band-gap and relative Fermi level (E_F) shifts for all possible Cur-NR and M–Cur-NR complexes with respect to the component control systems. A comparison of the total energy of the M–Cur-NR systems shows that Hg–Cur-NR and the Hg-bridge configurations are lowest in the total energies. In Table 4, the optimized distances between two moieties, as obtained after ionic relaxation, are listed, which suggests the

Table 3 Ground state energy per atom, HOMO LUMO energy, band gap and relative shift of E_F of the systems with respect to Cur/M–Cur or NR

Systems	Ground state energy/atom	Homo (eV), Lumo (eV)	Band-gap	Relative shift of E_F with respect to the Cur/M–Cur	Relative shift of E_F with respect to NR
NR	−3.95	−0.62, 2.24	2.86	—	—
Cur	−6.40	−0.90, 2.21	3.11	—	—
Zncur	−6.27	0.01, 3.88	3.87	0.88	NA
Hgcur	−6.40	0.0, 3.53	3.53	0.54	NA
Cur-NR	−5.67	−1.02, 1.33	2.35	−0.2	+1.36
Zncur-NR	−5.54	−0.62, 2.22	2.84	−0.86	+1.58
Hgcur-NR	−5.50	0.33, 3.10	3.10	−1.59	+0.51
Hg-bridge	−5.84	0.31, 3.19	3.19	−1.81	+0.29

2508 | *Phys. Chem. Chem. Phys.*, 2017, **19**, 2503–2513

This journal is © the Owner Societies 2017

highest distance for the Hg–Cur-NR system. This trend is qualitatively similar to the experimentally obtained FRET distances. It may be mentioned that for the configuration with Hg–Cur attached to the NR *via* the middle diketo moiety, large structural distortions of the NRs lead to a break-up of the Hg–Cur-NR assembly with the total energy of the system much higher than the stable configurations. Although, both Zn and Hg have d^{10} systems, the larger size of the Hg^{2+} ion is mostly responsible for such structural distortion induced increase in ground state energy. In addition, an investigation of the binding energies (BE) of the Cur/M–Cur-NR complexes reveals the fact that the order of decrease in BE of the systems are like: BE (Cur-NR) > BE (Zncur-NR) > BE (Hgcur-NR) > BE (Hg-bridge).

After the confirmation of the attachment between Cur or M–Cur and ZnO NR, photocurrent measurements were performed in the fabricated photovoltaic devices. Fig. 3a is the schematic representation of the fabricated device using Cur or M–Cur sensitized ZnO NR on FTO plates as the photoanode and Pt as the counter electrode and iodide/triiodide solution as the electrolyte. The photocurrent response signal for ZnO NR with different cur or M–Cur remains similar under UV irradiation but under 1 sun illumination, it follows an interesting trend as shown in Fig. 3b. An enhanced photocurrent was observed for the Hg–Cur (110 μA) compared to the ZnO NR (60 μA) whereas Cur and Zn–Cur show a reduced photocurrent (20 μA).

We have explored different photo-induced processes involved at the interfaces of the fabricated device to provide a detailed physical insight (Scheme 1). Upon light illumination, the Cur or M–Cur experienced photo-excitation. The excited state electrons are readily injected to proximal ZnO NR (Fig. S5 in the ESI†).
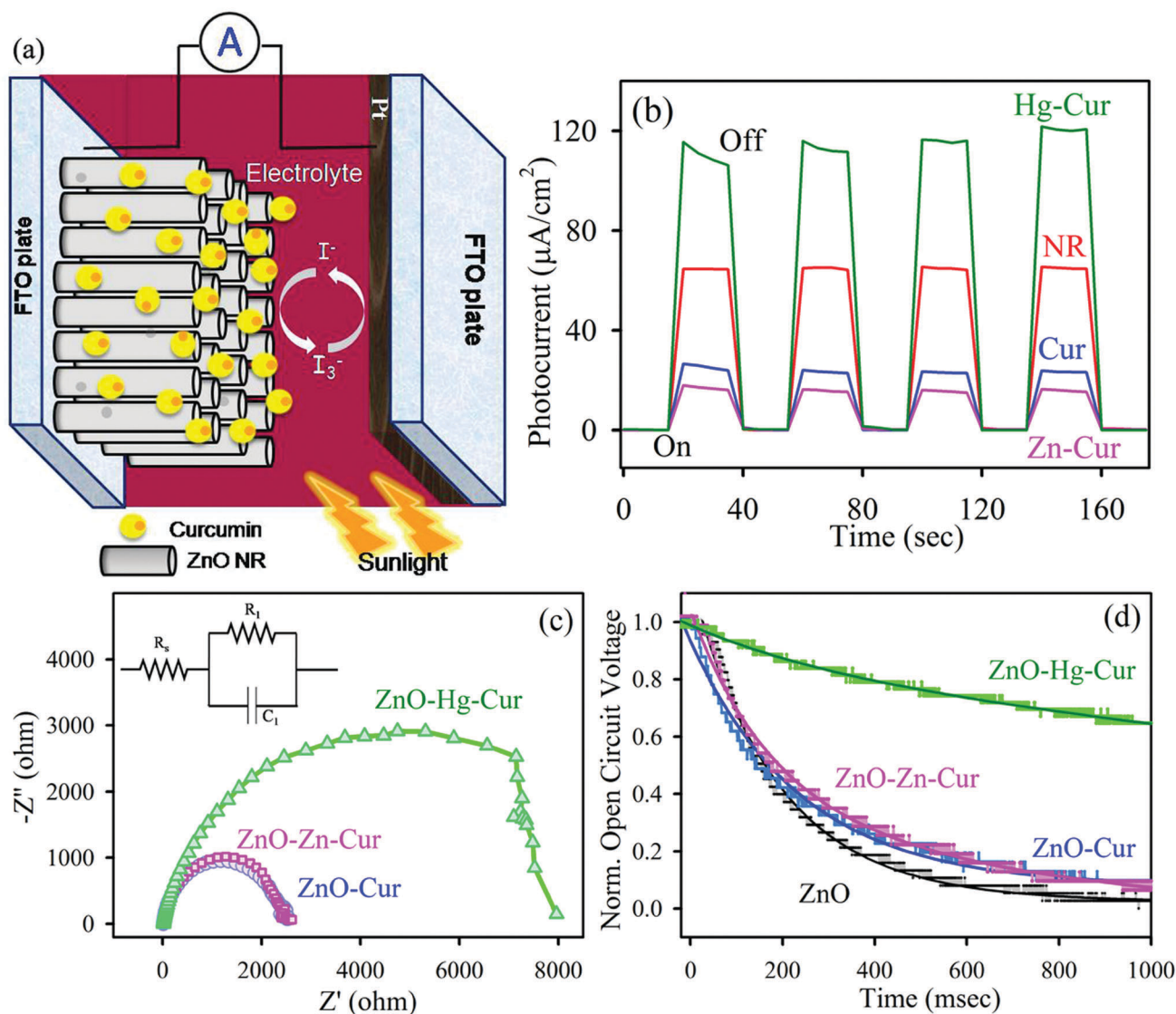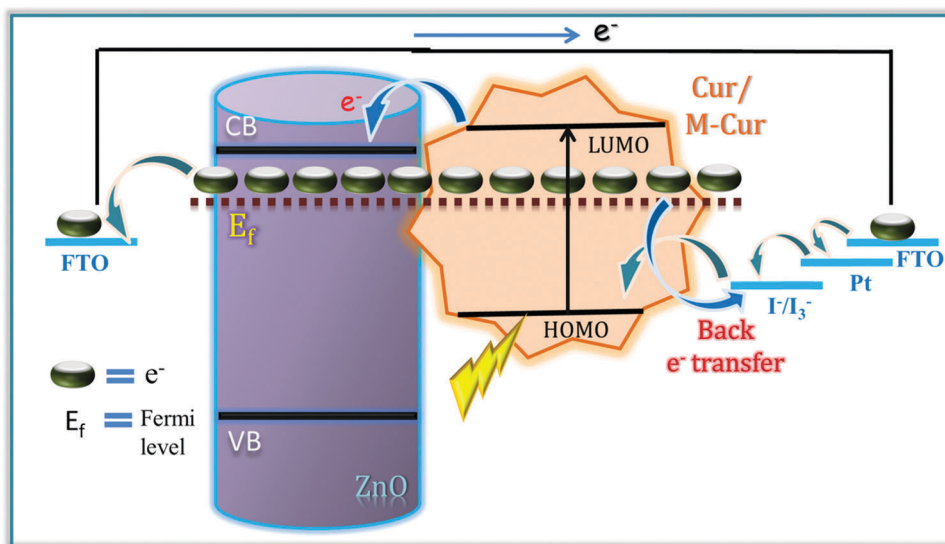

Fig. 3 (a) Schematic representation of photovoltaic device setup by using ZnO NRs fabricated on FTO as a working electrode and Pt as a counter electrode. Iodide-triiodide was used as electrolyte solution. (b) Photocurrent response of ZnO NR (red), ZnO–curcumin (blue), ZnO–Zn–curcumin (pink) and ZnO–Hg–curcumin (dark green). (c) Nyquist plots of different systems. Inset shows equivalent circuit model that was used to fit the EIS spectra. (d) Open circuit voltage decay profiles of different systems.

This journal is © the Owner Societies 2017

Phys. Chem. Chem. Phys., 2017, **19**, 2503–2513 | 2509

Scheme 1   Schematic representation of the ultrafast dynamic processes in ZnO-NR–Cur/M–Cur composites under light illuminated conditions.

These electrons are passing through external circuit and used for dye regeneration through an iodine redox couple.[47] But the interfacial back electron transport process from a Fermi level of an NR conjugated complex to an electrolyte and/or the charge recombination to HOMO of Cur or M–Cur plays a significant role in a photocurrent trend. Thus, to investigate these electronic and ionic processes, we use the electrochemical impedance spectroscopic (EIS) method.

As shown in Fig. 3c, the Nyquist plot features one semicircle, in the intermediate frequency region which is associated with the electron transport in the ZnO NR and back reaction at the NR conjugated complex/electrolyte interface.[48] The Nyquist plots are fitted using the equivalent circuit (where C_1 is capacitance and R is resistance) shown in the inset of the Fig. 3c and the parameters are summarized in Table 5. The R_1 value represents the interfacial recombination resistance at an NR conjugated complex/electrolyte interface and is much higher for Hg–Cur-NR than those of Cur-NR and Zn–Cur-NR. This suggests less charge recombination from the Hg–Cur-NR photo-anode to the triiodide ions in the electrolyte. The lifetime of accumulated charges at the photo-anode can be monitored by taking the decay of the open circuit voltage in the dark following a brief period of illumination. Upon visible light illumination, the excited Cur or M–Cur injects electrons into ZnO NR. The accumulated electrons in the Fermi level move to the more negative potential. The forward electron injection is terminated upon stopping the illumination, thus discharging of electrons occurs through the back electron transfer or

recombination with the oxidized electrolytes. The open circuit voltage decay reflects the timescales for the recombination processes. Fig. 3d shows the decay profiles of different systems. The fitted timescales are presented in Table 6. The Hg–Cur-NR photo-anode exhibits a remarkably slow rate of voltage decay (12.7 s) compared to the other systems. This can be attributed to peripheral attachment of Hg–Cur to NR which contributes in fewer electron recombination processes.

The atom (APDOS) and orbital-projected density of states (OPDOS) and the corresponding energy eigenvalues of the NR conjugated complexes are displayed in Fig. 4, along with the two control systems Cur and NR. Fig. 4a and b exhibit the total DOS of the Cur and NR systems with the respective highest occupied molecular orbital (HOMO) and lowest unoccupied molecular orbital (LUMO) levels. Both of these systems are found to be wide band gap semiconductors with some gap states because of the dangling bonds at the surface. In Fig. 4c, for the Cur-NR combined system, a shift of E_F with respect to the Cur and NR system is found to be 0.2 eV towards the valence band (VB) and 1.36 eV towards the conduction band (CB) respectively, implying a p(n)-type doping of the Cur(NR). This stipulates an obvious electron transfer from the Cur to NR system, complementing the experimental indication. The DOS figures also show a strong O-2p of Cur to NR Zn-3d hybridization, including the filled states at the top of the VB ($\sim$0.7 eV below E_F) as well as the empty gap states ($\sim$0.65 eV above E_F). Fig. 4d for the Zn–Cur-NR assembly unveils that the charge transferred from

Table 5   EIS parameters of fabricated photovoltaic device using different active electrodes

Active electrode	R_s (Ω)	R_1 (Ω)
ZnO-NR–Cur	14.09	2258
ZnO-NR–Zn–Cur	16.27	2283
ZnO-NR–Hg–Cur	13.44	3193

Table 6   Dynamics of photovoltage transients of fabricated photovoltaic device using different active electrodes

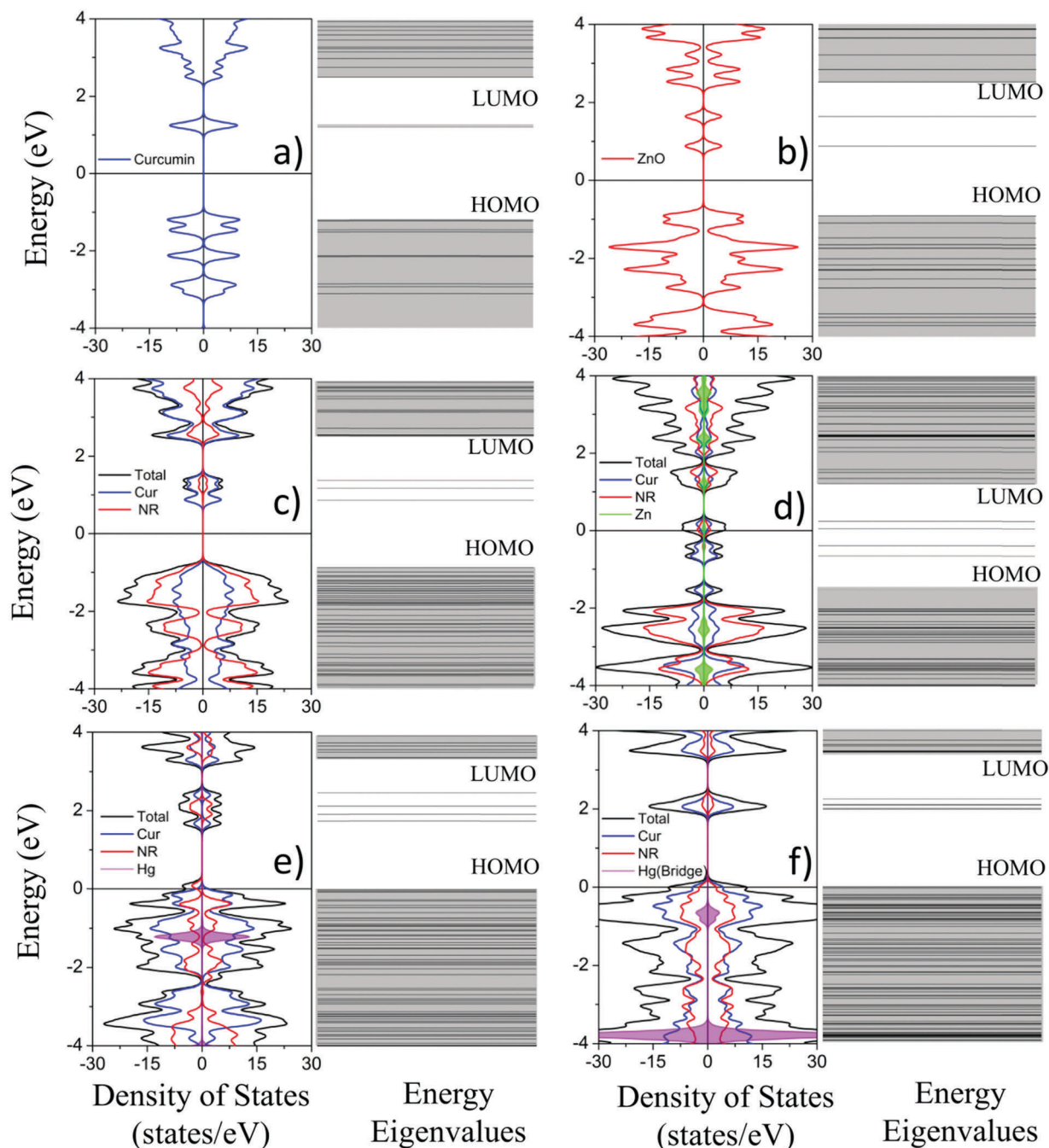| Active electrodes	τ_1 (ms)	τ_2 (ms)	τ_{avg} (ms)
ZnO NR	154.7 (50%)	230 (50%)	192.4
ZnO-NR–Cur	134.6 (55%)	552 (45%)	322.4
ZnO-NR–Zn–Cur	164 (59%)	711.6 (41%)	388.5
ZnO-NR–Hg–Cur	—	12699.5 (100%)	12699.5

Fig. 4 Atom (APDOS) and orbital (OPDOS) projected density of states (DOS) and the corresponding energy eigenvalues of (a) pure Cur, (b) pure ZnO NR, (c) Cur-NR, (d) Zn–Cur-NR, (e) Hg–Cur-NR and (f) Hg–Cur-NR (bridge).

Zn–Cur to NR fills up the empty O-2p dangling bond induced gap states both from Cur and NR, as present in 4c, keeping the NR Zn-3d and Zn–Cur Zn-3d levels partially filled at E_F and Zn-3d induced donor levels created within 0.1 eV of CB. In a similar way to Cur-NR, there is a p(n) type doping of the Zn–Cur-NR system, indicating a charge transfer from Zn–Cur to NR. A comparison with Fig. 4c shows more localized and increased intensity of VB NR-DOS in comparison to the Cur-NR system. The relative shifts of E_F with respect to the Zn–Cur and NR systems are -0.86 eV and 1.58 eV, respectively. In comparison to Cur-NR, there is only a

small shift of E_F by 0.22 eV towards CB in addition to a reduction of the HOMO–LUMO gap. Zn–Cur possesses almost similar E_F and a similar amount of the charge transfer from Zn–Cur to NR as the Cur-NR system. From Bader analysis, the amount of electron transfer from Cur/Zn–Cur to NR is $\sim$3e. This also explains the similar photocurrent behaviour for these two systems.

As compared to the Cur-NR and Zn–Cur-NR systems, Hg–Cur-NR systems are energetically more favourable, as can be seen from the ground state total energy normalized by the number of atoms presented in Table 3. The Hg-bridge structure

This journal is © the Owner Societies 2017

Phys. Chem. Chem. Phys., 2017, **19**, 2503–2513 | **2511**

is lowest in normalized ground state energy. Due to its larger ionic radii, Hg^{2+} introduces more buckling and structural distortions within the system. The buckling angle between central C atoms for Hg–Cur-NR is 7.4°, which is much higher than Cur-NR and Zn–Cur-NR (3.6° and 0.4° respectively). While comparing the Fermi level shifts, the large shift of the Hg–Cur Fermi-level towards the valence band for Hg–Cur-NR (−1.59 eV) and the Hg-bridge (−1.81 eV) indicates a huge charge transfer from Hg–Cur to NR for both of these configurations. Bader partitioning analysis implies that the charge transfer from the Hg–Cur to the NR can be quantified as ∼3e and ∼10e for the Hg–Cur-NR and Hg-bridge configuration respectively. This transferred charge renders the Fermi-level to shift within the valence band, imparting a metallic character within the system. The spin-polarized behaviour in the case of the Hg–Cur-NR system is subdued for the Hg-bridge system due to the symmetric nature of the charge transfer. In contrast to the Cur-NR and Zn–Cur-NR systems, inherent structural distortion of the Hg systems also generates NR and Hg–Cur induced shallow acceptor levels, which while overlapping with top of the VB are responsible for the metallic behaviour and better photocurrent for the Hg–Cur-NR systems.

5. Conclusions

In summary, we have designed a facile detection procedure based on ZnO NR to estimate and characterize heavy-metal conjugated curcumin. ZnO NR of 2–3 μm of length and 80–100 nm diameters were synthesised using a hydrothermal method and characterised using electron microscopy (SEM, HRTEM) and X-ray diffraction (XRD). Three samples were employed namely Cur (pure), Zn–Cur (non-toxic M–Cur) and Hg–Cur (toxic M–Cur) for electrochemical deposition on ZnO NR surface and attachment is confirmed by cyclic voltammetry studies. To confirm the proximity of the ZnO NR to Cur or M–Cur at the molecular level, we have employed picosecond-resolved Förster resonance energy transfer (FRET) from the defect mediated emission of ZnO NRs to Cur or M–Cur and the distance between the two is found to be dependent on the size of metal and the structure of the acceptor molecule. Computational investigation suggests variance of NR attachment sites due to the greater size of metal ions. We have fabricated a photovoltaic device based on molecular level interaction between ZnO and Cur or M–Cur, which shows a higher photocurrent for Hg–Cur. The EIS and open circuit voltage decay profiles show a remarkably slow rate of electron recombination from the Hg–Cur-NR photo-anode to the oxidized electrolyte. DOS analysis suggests metallic behaviour of Hg–Cur-NR compare to all other systems is reasonable for its higher photocurrent generation. This work is expected to find relevance for fabricating more selective and sensitive sensors to detect heavy-metal contamination in different herbal medicines.

Acknowledgements

References

1   D. S. Fabricant and N. R. Farnsworth, *Environ. Health Perspect.*, 2001, **109**, 69–75.
2   E. Haslam, T. H. Lilley, Y. Cai, R. Martin and D. Magnolato, *Planta Med.*, 1989, **55**, 1–8.
3   H. H. Fong, *Integrative cancer therapies*, 2002, **1**, 287–293, discussion 293.
4   K. Chan, *Chemosphere*, 2003, **52**, 1361–1371.
5   A. Michalak, *Pol. J. Environ. Stud.*, 2006, **15**, 523.
6   K. I. Priyadarsini, *Molecules*, 2014, **19**, 20091–20112.
7   B. B. Aggarwal, A. Kumar and A. C. Bharti, *Anticancer Res.*, 2003, **23**, 363–398.
8   C. D. Mock, B. C. Jordan and C. Selvam, *RSC Adv.*, 2015, **5**, 75575–75588.
9   Q. Wen, X. Zhang, J. Cai and P.-H. Yang, *Analyst*, 2014, **139**, 2499–2506.
10 F. Yang, G. P. Lim, A. N. Begum, O. J. Ubeda, M. R. Simmons, S. S. Ambegaokar, P. P. Chen, R. Kayed, C. G. Glabe, S. A. Frautschy and G. M. Cole, *J. Biol. Chem.*, 2005, **280**, 5892–5901.
11 W. Fu, W. Zhuang, S. Zhou and X. Wang, *Am. J. Transl. Res.*, 2015, **7**, 1189–1202.
12 S. Wanninger, V. Lorenz, A. Subhan and F. T. Edelmann, *Chem. Soc. Rev.*, 2015, **44**, 4986–5002.
13 X.-Z. Zhao, T. Jiang, L. Wang, H. Yang, S. Zhang and P. Zhou, *J. Mol. Struct.*, 2010, **984**, 316–325.
14 A. E. Schmitz, P. A. de Oliveira, L. F. de Souza, D. G. da Silva, S. Danielski, D. B. Santos, E. A. de Almeida, R. D. Prediger, A. Fisher, M. Farina and A. L. Dafre, *Biol. Trace Elem. Res.*, 2014, **158**, 399–409.
15 S. Ghosh, J. Kuchlyan, D. Banik, N. Kundu, A. Roy, C. Banerjee and N. Sarkar, *J. Phys. Chem. B*, 2014, **118**, 11437–11448.
16 D. Bagchi, S. Chaudhuri, S. Sardar, S. Choudhury, N. Polley, P. Lemmens and S. K. Pal, *RSC Adv.*, 2015, **5**, 102516.
17 W. R. Garcia-Nino and J. Pedraza-Chaverri, *Food Chem. Toxicol.*, 2014, **69**, 182–201.
18 K. Gleason, J. P. Shine, N. Shobnam, L. B. Rokoff, H. S. Suchanda, M. O. Ibne Hasan, G. Mostofa, C. Amarasiriwardena, Q. Quamruzzaman, M. Rahman, M. L. Kile, D. C. Bellinger, D. C. Christiani, R. O. Wright and M. Mazumdar, *J. Envtl Pub. Health*, 2014, **2014**, 730636.
19 C. G. Lin, L. A. Schaider, D. J. Brabander and A. D. Woolf, *Pediatrics*, 2010, **125**, e828–835.
20 L. Jarup, *British medical bulletin*, 2003, **68**, 167–182.
21 S. P. Dolan, D. A. Nortrup, P. M. Bolger and S. G. Capar, *J. Agric. Food Chem.*, 2003, **51**, 1307–1312.
22 S. Borowska and M. M. Brzoska, *J. Appl. Toxicol.*, 2015, **35**, 551–572.

23 Y. Jung, J. Lee, H. K. Kim, B. C. Moon, Y. Ji, D. H. Ryu and G.-S. Hwang, *Analyst*, 2012, **137**, 5597–5606.

24 B. Sunandan and D. Joydeep, *Sci. Tech. Adv. Mater.*, 2009, **10**, 013001.

25 R. J. Barnes, R. Molina, J. Xu, P. J. Dobson and I. P. Thompson, *J. Nanopart. Res.*, 2013, **15**, 1432.

26 Z. S. Seddigi, S. A. Ahmed, S. Sardar and S. K. Pal, *Sol. Energ. Mat. Sol. Cells*, 2015, **143**, 63–71.

27 S. Sardar, S. Chaudhuri, P. Kar, S. Sarkar, P. Lemmens and S. K. Pal, *Phys. Chem. Chem. Phys.*, 2015, **17**, 166–177.

28 S. Sarkar, A. Makhal, T. Bora, K. Lakhsman, A. Singha, J. Dutta and S. K. Pal, *ACS Appl. Mater. Interfaces*, 2012, **4**, 7027–7035.

29 R. Hariharan, S. Senthilkumar, A. Suganthi and M. Rajarajan, *Mater. Res. Bull.*, 2012, **47**, 3090–3099.

30 S. H. Kim, S. Y. Gwon, S. M. Burkinshaw and Y. A. Son, *Spectrochim. Acta Mol. Biomol. Spectrosc.*, 2010, **76**, 384–387.

31 P. Kar, S. Sardar, E. Alarousu, J. Sun, Z. S. Seddigi, S. A. Ahmed, E. Y. Danish, O. F. Mohammed and S. K. Pal, *Chem.–Eur. J.*, 2014, **20**, 10475–10483.

32 S. Chaudhuri, S. Sardar, D. Bagchi, S. S. Singha, P. Lemmens and S. K. Pal, *J. Phys. Chem. A*, 2015, **119**, 4162–4169.

33 J. R. Lakowicz, *Principles of Fluorescence Spectroscopy*, Springer US, 2007.

34 P. Singh, S. Choudhury, G. K. Chandra, P. Lemmens and S. K. Pal, *J. Photochem. Photobiol.*, 2016, **157**, 105–112.

35 S. Chaudhuri, S. Sardar, D. Bagchi, S. Dutta, S. Debnath, P. Saha, P. Lemmens and S. K. Pal, *ChemPhysChem*, 2016, **17**, 270–277.

36 G. Kresse and J. Hafner, *Phys. Rev. B*, 1993, **47**, 558.

37 S. Grimme, *J. Comput. Chem.*, 2006, **27**, 1787–1799.

38 X. Hou, L. Wang, G. He and J. Hao, *CrystEngComm*, 2012, **14**, 5158–5162.

39 M. A. Manaia, V. C. Diculescu, E. de Souza Gil and A. M. Oliveira-Brett, *J. Electroanal. Chem.*, 2012, **682**, 83–89.

40 G. Ziyatdinova, A. Nizamova and H. Budnikov, *J. Anal. Chem.*, 2012, **67**, 591–594.

41 R. N. Moussawi and D. Patra, *RSC Adv.*, 2016, **6**, 17256–17268.

42 A. Djurišić, Y. Leung, K. Tam, L. Ding, W. Ge, H. Chen and S. Gwo, *Appl. Phys. Lett.*, 2006, **88**, 103107.

43 K. Vanheusden, W. Warren, C. Seager, D. Tallant, J. Voigt and B. Gnade, *J. Appl. Phys.*, 1996, **79**, 7983–7990.

44 A. van Dijken, E. A. Meulenkamp, D. Vanmaekelbergh and A. Meijerink, *J. Phys. Chem. B*, 2000, **104**, 1715–1723.

45 S. K. Pal, J. Peon and A. H. Zewail, *Proc. Natl. Acad. Sci. USA*, 2002, **99**, 1763–1768.

46 K. K. Haldar, T. Sen and A. Patra, *J. Phys. Chem. C*, 2008, **112**, 11650–11656.

47 D. Cahen, M. Grätzel, J. F. Guillemoles and G. Hodes, *Electrochemistry of Nanomaterials*, Wiley-VCH Verlag GmbH, Weinheim, Germany, 2001, pp. 201–228.

48 Q. Wang, J.-E. Moser and M. Grätzel, *J. Phys. Chem. B*, 2005, **109**, 14945–14953.